Raman study of the coupling of crystal-field excitations to phonons in $NdBa_2Cu_3O_{7-\delta}$

E. T. Heyen, R. Wegerer, E. Schönherr, and M. Cardona
Max-Planck-Institut für Festkörperforschung, Heisenbergstrasse 1, D-7000 Stuttgart 80, Germany
(Received 28 May 1991)

A double peak observed near 300 cm^{-1} in the Raman and inelastic-neutron-scattering spectra of the high-T_c superconductor $NdBa_2Cu_3O_{7-\delta}$ is due to a strong coupling and mixing of the B_{1g}-symmetry Raman phonon and crystal-field (CF) excitations of the Nd^{3+} $4f$ electrons of the same symmetry. In this paper, we describe in detail a model based on the coupling of extended phonons and localized CF excitations. Higher phonon quantum numbers have to be taken into account at room temperature. We show that this interpretation is compatible with measurements of the dependence on temperature, oxygen isotopic substitution, laser wavelength, and oxygen content. We obtain from our model the CF-phonon coupling constant as well as the frequencies of the unperturbed phonon and CF excitation. We also discuss the breaking of the polarization selection rules for the highest phonon based on the substitution of Ba by Nd ions.

I. INTRODUCTION

Recently, Yoshida *et al.*[1] reported measurements of the Raman spectra of $NdBa_2Cu_3O_y$ single crystals. In addition to the five peaks that are usually observed in $RBa_2Cu_3O_7$ (R = rare earth) materials[2] they found at low temperatures a feature near 290 cm^{-1}. Usually, the five former peaks are assigned[2] to the five A_g-symmetry Γ–point phonons corresponding to a z-directed motion of the Ba, Cu(2) (plane copper), O(2)-O(3) (plane oxygen) out-of-phase, O(2)-O(3) in phase, and O(4) (apical oxygen) atoms. Yoshida *et al.*, however, suggest that the unexpected 290-cm^{-1} and the always detected 448-cm^{-1} modes correspond to the O(2)-O(3) A_g in-phase and O(4) x, y-directed B_{2g}, B_{3g} motions, respectively. They notice that the observation of the 448-cm^{-1} peak in zz polarization is not compatible with a B_{2g} or B_{3g} symmetry and attribute this forbidden Raman scattering to "Fröhlich-type interaction." Yoshida *et al.* also argue that the O(2)-O(3) in-phase mode should have a frequency similar to the out-of-phase phonon near 320 cm^{-1}. We just mention here that this latter argument does not hold, since it was recently shown by resonant Raman scattering[3] that the high frequency as well as the large zz-polarized intensity of the O(2)-O(3) in-phase mode near 448 cm^{-1} is due to strong admixture of O(4) motion.

We have previously demonstrated[4] that the assignment by Yoshida *et al.* is not compatible with our experimental data and that we can explain the Raman observations, as well as the detection of a similar double-peak structure in inelastic-neutron-scattering spectra by Allenspach *et al.*,[5] if we assume a strong coupling (and thus mixing) of the O(2)-O(3) out-of-phase phonon with a crystal-field (CF) excitation of slightly lower frequency. In particular, the surprising dependence on isotopic substitution and temperature follows from our model. A similar effect has been observed by inelastic neutron scattering[6] and interpreted[7,8] previously for the intermetallic cubic Laves-phase material $CeAl_2$.

In this paper, we present more experimental data and discuss in detail the theory that was only briefly sketched in Ref. 4. First, we describe the Raman-scattering spectra of $NdBa_2Cu_3O_{7-\delta}$ and their dependences on oxygen content, oxygen isotope, temperature, polarization, and laser wavelength and point out why the assignment of Yoshida *et al.* cannot be correct. In Sec. III we give an introduction to the crystal-field properties of the $4f$-electron states in $NdBa_2Cu_3O_{7-\delta}$. In Secs. IV and V, we describe in detail the model already outlined in Ref. 4 and calculate the Raman spectral function. We finally show in Sec. VI that we can explain our observations well within this picture. In Sec. VII, we discuss the unexpected polarization dependence of the O(4) phonon near 520 cm^{-1}.

II. EXPERIMENTAL RESULTS

We prepared $NdBa_2Cu_3O_7$ single crystals using K_2CO_3 as a flux.[9] Nd_2O_3, $BaCO_3$, K_2CO_3, and CuO were mixed with a molar ratio of 0.5:2.0:0.5:3.0, then heated in an alumina crucible for 3 days at 1060 °C, and finally cooled slowly (10 °C/h) to room temperature.[9]

The ceramic $NdBa_2Cu_3{}^{16}O_7$ samples were prepared by standard methods. The onset of strong diamagnetism was at T_c = 95 K according to susceptibility measurements. The oxygen concentration was determined to be $O_{7.0}$ by chemical analysis. Two of the ceramic samples were annealed for 115 h at 600 °C in an ^{18}O atmosphere. We know from gravimetric analysis that 86% of the ^{16}O was replaced by ^{18}O. Another ceramic sample was annealed for 16 h at 535 °C in vacuum in order to obtain nonsuperconducting $NdBa_2Cu_3O_{6.19}$, which we shall call, for simplicity, $NdBa_2Cu_3O_6$.

The Raman spectra were excited with the discrete lines of Ar^+ and Kr^+ lasers, dispersed with a SPEX triple monochromator and recorded with an ITT Mepsicron multichannel system.

The polarized Raman spectra of the $NdBa_2Cu_3O_7$ single crystal at 10 K are shown in Fig. 1. We use the Porto

notation $i(jk)l$ for the polarization geometry, where i and l denote the direction and j and k the polarization of incident and scattered light, respectively. x' and y' are rotated by 45° with respect to x and y around the z axis. Three peaks at 142, 172, and 442 cm^{-1} are observed in $z(xx)\bar{z}$ and $z(x'x')\bar{z}$, but neither in $z(x'y')\bar{z}$ nor in $z(xy)\bar{z}$ geometry, whereas both peaks of the structure near 300 cm^{-1} (which are the main subject of this paper) are detected in $z(xx)\bar{z}$ and $z(x'y')\bar{z}$ but not in $z(x'x')\bar{z}$ and $z(xy)\bar{z}$ configuration. The broad peak at 555 cm^{-1}, usually attributed to the O(4) phonon, is observed in all polarization geometries; it hence does not obey any specific selection rules. The origin of this peculiarity will be discussed in Sec. VII.

Since the environment of rare-earth atoms and the CuO_2 planes is nearly tetragonal, we will describe the symmetries of elementary excitations approximately within the tetragonal group D_{4h} $(4/mmm)$. While in the orthorhombic group D_{2h} (mmm) all peaks except that at 555 cm^{-1} belong to the fully symmetric A_g representation, they have, according to the specific selection rules mentioned above, different symmetries in the D_{4h} group: B_{1g} for the peaks at 274 and 331 cm^{-1} and A_{1g} for the three others. The 274-cm^{-1} mode hence cannot correspond to the O(2)-O(3) in-phase motion (as suggested by Yoshida *et al.*[1]), since it does not have A_{1g} but rather B_{1g} symmetry.

Figure 2 shows the dependence of the double-peak structure on temperature in the $NdBa_2Cu_3O_7$ single crystal. When the temperature increases, the higher mode shifts to lower frequencies by 17 cm^{-1}, while the *lower* peak decreases in intensity and shifts to higher frequencies. At room temperature the structure becomes very broad and asymmetric. There is still spectral weight at the frequencies of the low-temperature peaks, and there also seems to exist some substructure. For the ceramic sample of the same composition (Fig. 3) the overall behavior is similar; the low-temperature splitting between the two peaks, however, amounts only to 52 cm^{-1} as opposed to 57 cm^{-1} for the single crystal.

It can be seen in Fig. 4 that this behavior remains essentially unchanged in antiferromagnetic, insulating $NdBa_2Cu_3O_6$. This observation indicates that the appearance of the double-peak structure is not connected with the existence of the chains. However, the room-temperature width is much smaller than that for the fully oxygenated samples; also the lower peak appears to shift little with varying temperature while the higher mode shifts as much as in $NdBa_2Cu_3O_7$.

For a $NdBa_2Cu_3{}^{18}O_7$ sample, however, the temperature dependence is very different (Fig. 5): When cooling down from room temperature, a peak begins to grow on the *high*-frequency side. The splitting of the peaks is similar to the case of ^{16}O (Fig. 3); the isotopic shift at room temperature is 20 cm^{-1}, i.e., 6.3%; at 10 K, both peaks shift by only $\approx$ 11 cm^{-1}, i.e., 3.4% as compared to 6.0% expected for conventional one-phonon excitations and complete isotopic substitution. The tremendous high-temperature broadening as well as the unusual line shape are, however, still similar to the case of ^{16}O.

The relative intensities of the two peaks as well as their symmetry properties do not depend on the laser wave-

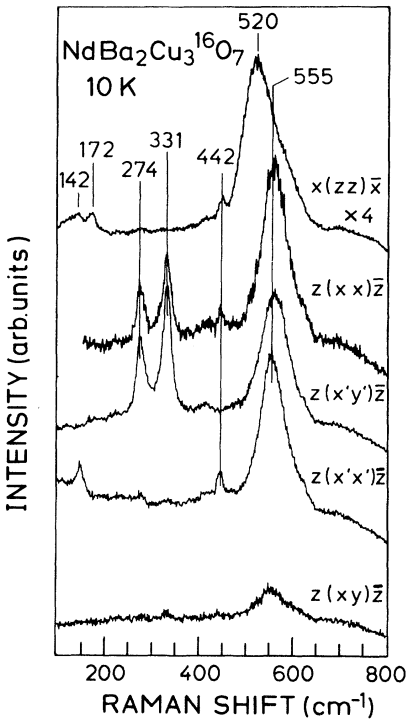

FIG. 1. Polarized Raman spectra at 10 K of a $NdBa_2Cu_3{}^{16}O_7$ single crystal.

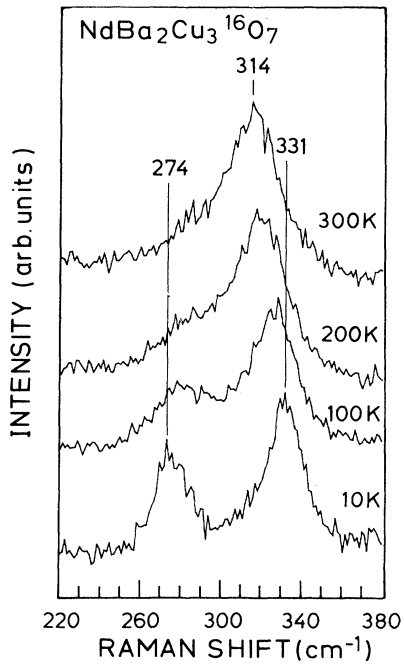

FIG. 2. Temperature dependence of the Raman spectra of a $NdBa_2Cu_3{}^{16}O_7$ single crystal in $z(xx)\bar{z}$ configuration. The lower panel shows the result of Lorentzian fits to the double-peak spectra. The dashed lines represent theoretical curves according to Eqs. (5) and (8) (see Sec. IV).

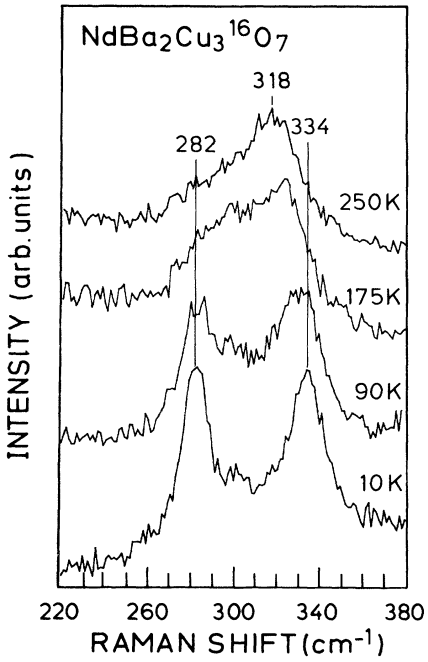

FIG. 3. Temperature dependence of the Raman spectra of a $NdBa_2Cu_3{}^{16}O_7$ ceramic sample.

length, as was shown by measurements at 10 K with $\lambda = 6471$, $\lambda = 5145$, and $\lambda = 4765$ Å (Fig. 6). These intensities, however, change strongly with respect to the other phonons.[3] This indicates that the mechanisms inducing the intensities of the two peaks are closely related.

In summary (i) we observed a double peak with clear B_{1g} (D_{4h}) symmetry, (ii) the splitting between both peaks decreases with increasing temperature, (iii) it appears also in insulating $NdBa_2Cu_3O_6$ and hence is not

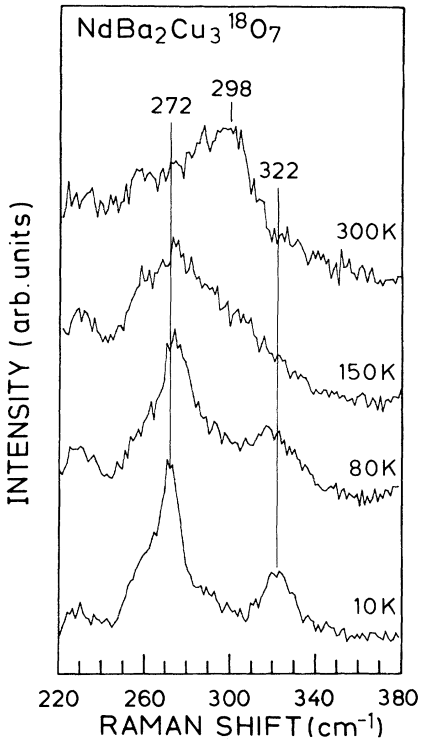

FIG. 5. Temperature dependence of the Raman spectra of a $NdBa_2Cu_3{}^{18}O_7$ ceramic sample.

related to the chains; the dependence of the broadening on temperature is different in this case, (iv) at room temperature the lower peak vanishes for ^{16}O samples, while the upper one does so for the ^{18}O-substituted samples, (v) the isotopic shift also depends on temperature, and (vi) the shape of the two peaks and their relative in-

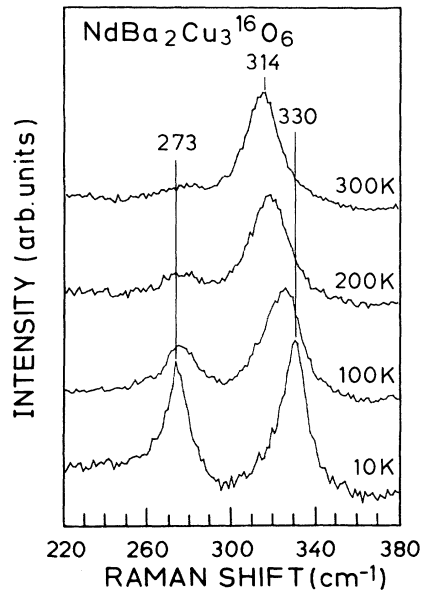

FIG. 4. Temperature dependence of the Raman spectra of a $NdBa_2Cu_3{}^{16}O_6$ ceramic sample.

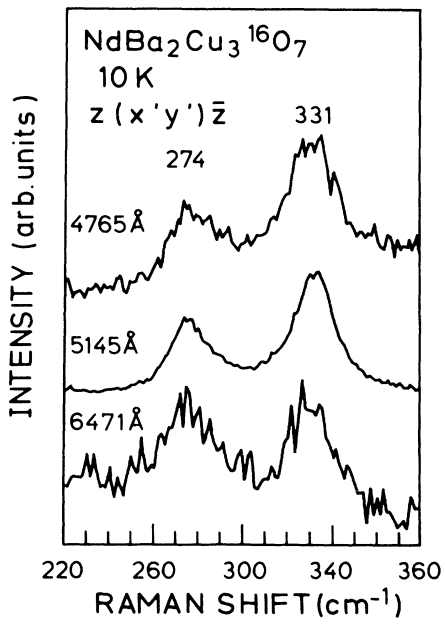

FIG. 6. Dependence of the Raman spectra of a $NdBa_2Cu_3{}^{16}O_7$ ceramic sample on laser wavelength.

tensities do not depend on resonance conditions; their intensities thus have a closely related origin.

III. CRYSTAL-FIELD EXCITATIONS IN $NdBa_2Cu_3O_{7-\delta}$

Before we proceed with the explanation of our results we describe the influence of the crystal field on the Nd^{3+} $4f$ electrons and the symmetries of the expected crystal field excitations.

Triply ionized rare-earth atoms have between 0 (Y^{3+}, La^{3+}) and 14 (Lu^{3+}) electrons in their $4f$ states. The spin-orbit (LS) coupling of these electrons leads to the formation of $^{2S+1}L_J$ configurations, each of which are $(2J+1)$-fold degenerate. The ground state of the three $4f$ electrons in Nd^{3+} is $^4I_{9/2}$ and is thus tenfold degenerate. The energy of the next-highest state $^4I_{11/2}$ is about 2000 cm^{-1} higher.[10] Note that each level characterizes the many-body state of the $4f$ electrons in one atom. Exactly one of the possible states (or a linear combination of the degenerate states, respectively) is occupied. (This picture is rather different from that of a Fermi liquid occurring in the valence bands of a metal.) Boltzmann statistics govern the occupation of those levels.

If a rare-earth atom is inserted in an environment of nonspherical symmetry, the degeneracy of the ground state is lowered. For an odd number of electrons the split states will remain at least doubly degenerate unless an external magnetic field is applied (Kramers rule).[10] The possible states can be characterized by their symmetry according to standard group theory. In the case of Kramers degeneracy the use of double groups[11] is required to take into account the transformation properties of spinors. The lowering of the angular-momentum degeneracy by cubic crystal fields (point group O_h) was calculated for all rare earths by Lea, Leask, and Wolf.[12] For Nd^{3+}, one finds that the $^4I_{9/2}$ ground state splits into a Γ_6^- Kramers doublet and two fourfold-degenerate Γ_8^- states. (Fig. 7, notation Ref. 11). All states have odd parity due to the odd number of f electrons. If the symmetry is lowered to tetragonal D_{4h}, the Γ_8^- states split into an M_6^- and an M_7^- doublet each, while the Γ_6^- (O_h) state is now called M_6^- (D_{4h}). If the symmetry is further lowered to orthorhombic D_{2h}, no additional splitting can occur according to Kramers' rule; now all states have the symmetry M_6^- (D_{2h}). In D_{2h}, no other symmetry exists for doublets. The lowering of the symmetry is sketched in Fig. 7.

Excitations between two possible $4f$ states $|i\rangle$ and $|j\rangle$ can be considered as quasiparticles (bosons) in a solid containing the rare-earth atoms. Their symmetry is the direct product of the representations of $|i\rangle$ and $|j\rangle$. We obtain

$$\begin{aligned} D_{4h}: \quad & M_6^- \times M_6^- = M_7^- \times M_7^- = A_{1g} + A_{2g} + E_g, \\ & M_6^- \times M_7^- = M_7^- \times M_6^- = B_{1g} + B_{2g} + E_g, \\ D_{2h}: \quad & M_6^- \times M_6^- = A_g + B_{1g} + B_{2g} + B_{3g}. \end{aligned} \tag{1}$$

These excitations are Raman active if they transform like components of a second-rank tensor (D_{4h} point group—

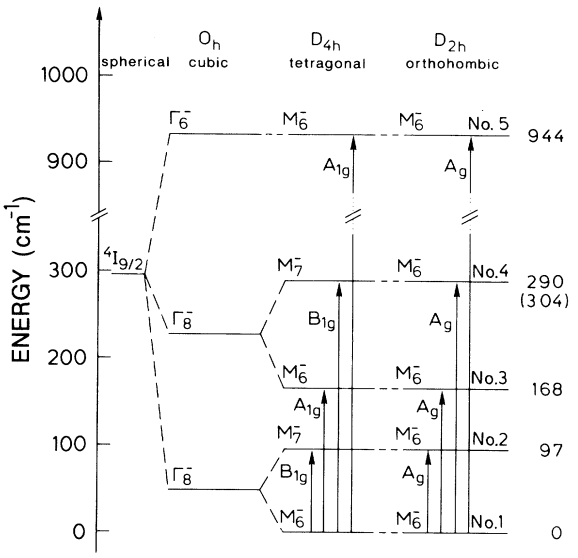

FIG. 7. Schematic plot of the five crystal-field doublet levels (No. 1,...,No. 5), their symmetries, and the symmetries of the Raman-active transitions for a Nd^{3+} ion in a spherical, cubic, tetragonal, and orthorhombic environment. Energies in cm^{-1} are the peak positions as observed in inelastic-neutron-scattering spectra (Ref. 14). The energy of the unperturbed fourth level as obtained from our model is also given in brackets.

$A_{1g}: x^2+y^2, z^2$; $B_{1g}: x^2-y^2$; $B_{2g}: xy$; $E_g: xz, yz$). They can also be measured by inelastic neutron scattering provided they transform like components of the angular-momentum operator $\mathbf{J}$ ($A_{2g}: J_z$; $E_g: J_x, J_y$ in tetragonal D_{4h} notation). Experimentally, one can distinguish between neutron scattering by phonons or CF excitations, since the cross section for CF scattering is proportional to $F^2(Q)|\langle i|\mathbf{J}|j\rangle|^2$, where the form factor $F(Q)$ has its maximum at $Q=0$.[13] This is very different from inelastic neutron scattering by phonons, which is proportional to Q^2.

Such crystal-field excitations in $RBa_2Cu_3O_{7-\delta}$ have been measured by inelastic neutron scattering for $R=$ Pr,[5,14] Nd,[5,14] Dy,[15] Ho,[16] and Er.[17] For $NdBa_2Cu_3O_7$, Goodman, Loong, and Soderholm[14] find crystal-field-split levels at 0, 97, 168, 290, and 944 cm^{-1}. The symmetry assignments (M_6^-) have only been performed for the orthorhombic D_{2h} group. Table 3 of Ref. 14, however, also gives the calculated magnetic transition strengths μ for $\mathbf{J} \parallel z$ ($\mu_\parallel$) and $\mathbf{J} \perp z$ ($\mu_\perp$) polarization configurations. We showed above that $M_6^- \leftrightarrow M_7^-$ transitions have, in the tetragonal group D_{4h}, no A_{2g} component, and hence $\mu_\parallel = 0$. There is no selection rule for $\mu_\perp$, since the E_g representation is present in $M_6^- \leftrightarrow M_6^-$ as well as $M_6^- \leftrightarrow M_7^-$ transitions. Using the fact that for $M_6^- \leftrightarrow M_7^-$ transitions $\mu_\parallel$ should then be almost zero in the actual orthorhombic symmetry, we can thus quickly derive from Table 3 of Ref. 14 the D_{4h} symmetries, which are also given in Fig. 7. (Here we had to ignore the calculated μ for transitions from the ground level to the

first excited level, which are one or two orders of magnitude weaker than the other transitions.) We find from the neutron experiments that at zero temperature, when only the M_6^- (D_{4h}) ground level is occupied, there exist two Raman-active crystal-field excitations with B_{1g}, B_{2g}, and E_g symmetry (D_{4h}) at 97 and 290 cm^{-1} and two others with A_{1g}, A_{2g}, and E_g symmetry at 168 and 944 cm^{-1} (Fig. 7).

IV. THE COUPLED-PHONON–CRYSTAL-FIELD EXCITATIONS

Two elementary excitations having the same symmetry may couple leading to a renormalization of the quasiparticles yielding changes of frequencies, line widths, and eigenvectors, depending on the coupling strength. Since the plane oxygen atoms are the nearest neighbors of the Nd^{3+} ions, it is likely that a plane oxygen phonon modulates the crystal field and thus the CF split levels significantly. The renormalization effects are maximized if the energy difference of the participating elementary excitations is small as can be seen, e.g., from perturbation theory of any order. Observable effects may therefore only be expected if a CF transition has an energy similar to that of one of the two Raman active plane oxygen phonons. In addition, the CF excitation and the phonon must have the same symmetry in the tetragonal group D_{4h}. A process that is symmetry forbidden in D_{4h} will not have significant strength in the actual orthorhombic (D_{2h}) case, although it will then formally be an allowed process.

All these conditions are accidentally fulfilled in $NdBa_2Cu_3O_{7-\delta}$ for the B_{1g} CF excitation and the B_{1g} phonon near 300 cm^{-1}. In second-quantized notation, the corresponding Hamiltonian may be written as

$$
\begin{aligned}
&H = H_0 + H_1, \\
&H_0 = \hbar\omega_{\mathrm{ph}}\left(aa^\dagger + \frac{1}{2}\right) + \sum_{l=1,4;m} \hbar\omega_{\mathrm{CF}}(l) c_{lm} c_{lm}^\dagger, \qquad (2) \\
&H_1 = V \sum_{m'm} (a + a^\dagger)(c_{1,m} c_{4,m'}^\dagger + c_{1,m}^\dagger c_{4,m'}),
\end{aligned}
$$

where we consider only the B_{1g} phonon (creation operator $a^\dagger$) and the relevant first and fourth CF states (creation operators $c_1^\dagger$ and $c_4^\dagger$, respectively. We ignore the dispersion in $\mathbf{k}$ space. m, m' are the degeneracy indices running from 1 to 2. H_0 is the unperturbed Hamiltonian and H_1 represents the lowest-order coupling neglecting anharmonic processes.

At zero temperature, all Nd^{3+} ions are in the M_6^- ground state and no phonons are thermally excited. We can then easily calculate the renormalization following Thalmeier and Fulde.[7] We consider the four-dimensional subspace spanned by the state $|M_7^-, 0\rangle$ (CF configuration being only in one unit cell in the excited M_7^- state, phonon quantum number zero) and $|M_6^-, 1\rangle$ (all CF configurations in the ground state, quantum number 1 for the B_{1g} phonon). The latter state has also M_7^- symmetry, since $M_6^- \times B_{1g} = M_7^-$. Hence both states are doubly degenerate, this degeneracy persisting in the case of coupling. We assume that all other CF levels are not significantly affected by the renormalization, since either the respective energy denominators are too large or the coupling is symmetry forbidden. One obtains[7] for the two renormalized energies by exact diagonalization of the Hamiltonian the eigenenergies

$$
E_{1,2} = \frac{\hbar(\omega_{\mathrm{ph}} + \omega_{\mathrm{CF}})}{2} \pm \sqrt{\left(\frac{\hbar(\omega_{\mathrm{ph}} - \omega_{\mathrm{CF}})}{2}\right)^2 + \frac{V^2}{2}}, \qquad (3)
$$

yielding two M_7^- states both allowing transitions of B_{1g} symmetry from the ground state [Eq. (1)].

Thalmeier and Fulde[7,8] showed that this picture remains unchanged even when phonon dispersion is taken into account provided that the phonon band width $\hbar\omega_b$ is smaller than V. This condition is most likely fulfilled for $NdBa_2Cu_3O_{7-\delta}$, where the splitting is ≈ 50 cm^{-1} at low temperature, while the width for this particular phonon band should be approximately 15 cm^{-1} (the band minimum being at the Γ point), the value for the isostructural $YBa_2Cu_3O_7$ as obtained from inelastic-neutron-scattering experiments.[18] In this case the phonon-like continuum will persist undisturbed and the two M_7^- states (CF excitation and phonon at $\mathbf{k} = \mathbf{0}$) will be pushed above and below the continuum.

At nonzero temperature, the picture is considerably more complicated, since all CF levels are occupied in the different unit cells according to Boltzmann statistics so that not in every unit cell is a B_{1g} transition from the first to the fourth level possible. The phonons that are created by the Stokes Raman-scattering process extend over many unit cells and hence interact with randomly distributed localized CF excitations. For example, while at zero temperature the occupation probability p_1 for each of the two degenerate ground states is 0.5 and $p_2 = p_3 = p_4 = p_5 = 0$, we have at 300 K $p_1 = 0.21$, $p_2 = 0.13$, $p_3 = 0.10$, $p_4 = 0.05$, and $p_5 = 0.00$. If we call P_n the probability of having a phonon state with quantum number n, we find at zero temperature $P_0 = 1$, $P_1 = P_2 = \cdots = 0$ and at 300 K $P_0 = 0.77$, $P_1 = 0.18$, $P_2 = 0.04$, $P_3 = 0.01$, etc. At elevated temperature, higher phonon quantum numbers also become relevant.

At lowest order, the Hamiltonian [Eq. (2)] leads to the two Feynman diagrams for the phonon self-energy given in Fig. 8. In both cases the initial state $|n, 0>$ is the superposition of a phonon state with quantum number n and a CF level distribution $p_1, p_2, \ldots, p_5$ in thermal equilibrium. This state can then undergo a virtual transition to another state $|n+1, -_j>$ [Fig. 8(a)] by relaxing the CF configuration in the jth unit cell, which has been excited in the fourth level before, to the ground state and by simultaneously emitting one phonon. There, hence, exist $p_4 N$ different $|n+1, -_j>$ states with N being the number of unit cells in the crystal. The matrix element for this vertex is

$$
\begin{aligned}
< n, 0|H_1|n+1, -_j > &= V < n, 0|ac_1 c_4^\dagger|n+1, -_j > \\
&= V\sqrt{n+1}. \qquad (4)
\end{aligned}
$$

In second-order perturbation theory this diagram

yields a self-energy,

$$+\frac{V^2(n+1)}{\omega_{\rm ph}-\omega_{\rm CF}}, \tag{5}$$

The other graph [Fig. 8(b)] shows the transition from the $|n,0>$ state to the $|n-1,+_k>$ state having a phonon quantum number $n-1$ and the kth unit cell (previously being in the ground state) excited in the fourth CF state. There are p_1N different $|n-1,+_k>$ states. The matrix element is in this case

$$\begin{aligned} <n,0|H_1|n-1,+_k> &= V<n,0|a^\dagger c_1^\dagger c_4|n-1,+_k> \\ &= V\sqrt{n} \end{aligned} \tag{6}$$

yielding a self-energy,

$$-\frac{V^2 n}{\omega_{\rm ph}-\omega_{\rm CF}}. \tag{7}$$

Since at low temperature [Eq. (3)] the matrix element V is larger than the splitting $\omega_{\rm ph}-\omega_{\rm CF}$, we are in the strong-coupling limit and second-order perturbation theory does not apply. Instead, we have to sum up all possible sequences of the two Feynman diagrams, this being equivalent to the exact diagonalization of the Hamiltonian for the Hilbert subspace under consideration.

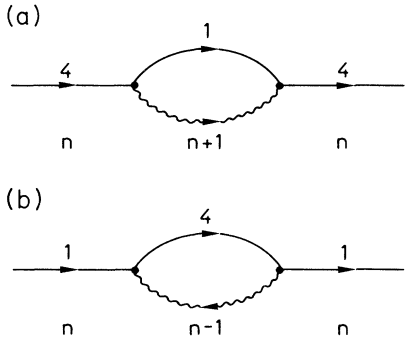

FIG. 8. Lowest-order Feynman diagrams describing the self-energy of a phonon (wavy line) interacting with transitions between the first and fourth crystal-field levels (solid lines). The actual phonon quantum number of the system is indicated below.

In principle, we would have to consider as a basis the p_4N different states $|n+1,-_j>$ ($j=0,1,\ldots,p_4N-1$), the initial state $|n,0>$ for a phonon excitation at a certain **k** point, and the p_1N different states $|n-1,+_k>$ ($k=0,\ldots,p_1N-1$). The coupling Hamiltonian is then

$$H_1^n=\frac{V}{\sqrt{N}}\begin{pmatrix} & & & \sqrt{n+1} & & & \\ & & & \vdots & & & \\ \sqrt{n+1} & \cdots & \sqrt{n+1} & \sqrt{n+1} & \sqrt{n} & \cdots & \sqrt{n} \\ & & & 0 & & & \\ & & & \sqrt{n} & & & \\ & & & \vdots & & & \\ & & & \sqrt{n} & & & \end{pmatrix}. \tag{8}$$

(The coupling matrix element V does, in general, for every unit cell, have a different complex phase. Only for phonons at **k**=0, which are created by the Raman scattering process, this phase is constant and can hence be ignored).

This expression can be simplified by a basis transformation which reorders the phases only within the subspaces of the $|n-1,+_k>$ and $|n+1,-_j>$ states, respectively:

$$\begin{aligned} |n-1,\alpha> &= \frac{1}{p_1N}\sum_{k=0}^{p_1N-1}\exp\left(2\pi i\frac{k\alpha}{p_1N}\right)|n-1,+_k>, \quad \alpha=0,1,\ldots,p_1N-1, \\ |n+1,\beta> &= \frac{1}{p_4N}\sum_{j=0}^{p_4N-1}\exp\left(2\pi i\frac{j\beta}{p_4N}\right)|n+1,-_j>, \quad \beta=0,1,\ldots,p_4N-1. \end{aligned} \tag{9}$$

When transforming the coupling Hamiltonian H_1, all terms for $\alpha\neq 0$ and $\beta\neq 0$ vanish, since the complex exponential terms average to zero. In the reduced basis consisting only of $|n+1,\beta=0>$, $|n,0>$, and $|n-1,\alpha=0>$ states the Hamiltonian finally becomes

$$H_1^n=V\begin{pmatrix} & \sqrt{(n+1)p_4} & \\ \sqrt{(n+1)p_4} & & \sqrt{np_1} \\ & \sqrt{np_1} & \end{pmatrix}. \tag{10}$$

With $(n+1)\omega_{\rm ph}-\omega_{\rm CF}$, $n\omega_{\rm ph}$, and $(n-1)\omega_{\rm ph}+\omega_{\rm CF}$ being the energies of the three basis states, we can now diagonalize the Hamiltonian for every n,

$$H^n=H_0^n+H_1^n, \tag{11}$$

with

$$H_0^n=\begin{pmatrix} (n+1)\omega_{\rm ph}-\omega_{\rm CF} & & \\ & n\omega_{\rm ph} & \\ & & (n-1)\omega_{\rm ph}+\omega_{\rm CF} \end{pmatrix}. \tag{12}$$

The eigenstates $|1^n>$, $|2^n>$, $|3^n>$ and eigenenergies E_1^n, E_2^n, E_3^n have the following properties.

(i) At low temperatures, when $p_1 = 1$ and $p_4 = 0$, the Hamiltonian reduces to the two-level system discussed above [Eq. (3)], i.e., we have a strong mixing involving only the $|\alpha = 0>$ and the $|\mathrm{ph}>$ state, while the $|\beta = 0>$ state remains unaffected.

(ii) At elevated temperature, the splitting between the two low-temperature peaks decreases (since p_1 decreases), while the mixing and splitting with the $|\beta = 0>$ state increase.

(iii) Since $\sqrt{n}$ or $\sqrt{n+1}$ appear in the matrix, the coupling strength, and hence the mixing and splitting, increase with increasing phonon quantum number n.

How is this picture influenced if the phonon dispersion is taken into account? As pointed out by Thalmeier,[8] the CF excitation interacts with the whole phonon band still leading to two poles in the spectral function provided that the coupling is large enough to push both peaks out of the phonon continuum. Otherwise, the peaks broaden strongly, since the CF excitation can then decay into the continuum. In order to concentrate on the temperature dependence, we have so far ignored the phonon dispersion. At low temperature this is correct, since the splitting is large enough.

We now have to take into account that the coupling matrix V is some average over the Brillouin zone. For instance, at the zone edge the phonon has E rather than B_{1g} local character around the rare-earth atom and couples more to the E_g component of the CF excitation [Eq. (1)]. This could have the consequence that V peaks around $\mathbf{k} = \mathbf{0}$. In addition, this average is weighted by the phonon density of states (PDOS) being approximately two dimensional. Since the phonon dispersion has only been measured[18] on twinned crystals, it is *a priori* not clear if the PDOS singularity at the Γ point is a step function or a logarithmic divergence, but the latter may obtain, thus enhancing the weight of $\mathbf{k} = \mathbf{0}$ phonons in the coupled excitations.

At elevated temperature, however, when the two main peaks approach each other and also other transitions become allowed, these transitions will decay into the phonon continuum. As a consequence, the CF excitations, which are the intermediate states in the diagrams used for the calculation of self-energies (Fig. 8) will broaden and the effective coupling is expected to decrease. The structure then should more closely resemble the uncoupled case than predicted by Eqs. (10)–(12).

V. THE RAMAN SPECTRAL FUNCTION

Since in none of the R-1:2:3 (R = rare earth) materials have CF excitations been previously identified in the Raman spectra [although they are, in principle, Raman-allowed according to Eq. (1)], we conclude that the cross sections for Raman scattering by CF excitations can be neglected in comparison to those of Raman scattering by phonons. Via the coupling and mixing, the CF transitions acquire phononic character; they are therefore observable. This premise is confirmed by the fact that the intensity ratio of the double peak does not depend on laser wavelength, i.e., resonance conditions (Fig. 6), although the intensities of the individual components change substantially relative to the other phonons.[4] This indicates that the same mechanism must be responsible for the intensity of both components of the doublet.

From the diagonalization of the Hamiltonian [Eqs. (10)–(12)] we obtain the eigenvector matrix α_{ij}^n, connecting the renormalized states $|i^n>$ with the unperturbed states $|j^n>'$, where $|j^n = 1>'$ is the $|n+1, \beta = 0>$ state, $|j^n = 2>'$ is the $|n, 0>$ state, and $|j^n = 3>'$ is the $|n-1, \alpha = 0>$ state. All transitions from the states $|j^n>$ to the states $|i^{n+1}>$ contribute to the spectral function, weighted with the "phonon contents" α_{i2}^{n+1} and α_{j2}^n of the participating states, respectively, and also with the probability P_n for an n-phonon state being occupied and with the general $(n+1)$-factor always present for Stokes scattering.[19] We assume every transition to have a Lorentzian line shape $L(E_i^{n+1} - E_j^n, \Gamma_{ij})$ centered at the energy $E_i^{n+1} - E_j^n$ with a half width at half maximum Γ_{ij} .

We obtain the final result for the Raman spectrum $R(\omega)$

$$R(\omega) = \sum_{n=0}^{\infty} \sum_{i,j=1}^{3} P_n (n+1)(\alpha_{i2}^{n+1} \alpha_{j2}^n)^2 L(E_i^{n+1} - E_j^n, \Gamma_{ij}). \tag{13}$$

Γ_{ij}, being proportional to the imaginary part of the coupling self-energy, may, in principle, vary for different i, j.

VI. DISCUSSION

First, we determine the unrenormalized frequencies ω_{ph}, ω_{CF}, and the CF–phonon coupling constant V, which enter the Hamiltonian in Eqs. (11) and (12) from the low-temperature spectra for the ceramic $NdBa_2Cu_3{}^{16}O_7$ sample (Fig. 3). The intensity ratio of the doublet as well as the two frequencies contain enough information to determine the three parameters. If $\omega_{\mathrm{ph}} = \omega_{\mathrm{CF}}$ were true, we would always have a 50%-50% mixing and both peaks would have the same intensity. The degree of mixing decreases with increasing $\omega_{\mathrm{ph}} - \omega_{\mathrm{CF}}$. The choice of parameters is further restricted, since, according to Eq. (3), which is equivalent to Eqs. (10)–(13) at zero temperature, the centroid does not depend on the mixing so that $\omega_{\mathrm{ph}} + \omega_{\mathrm{CF}} = 282 + 334 = 616\ \mathrm{cm}^{-1}$. The matrix element is mainly determined by the splitting of $334 - 282 = 52\ \mathrm{cm}^{-1}$. We obtain the following parameters:

$$\begin{aligned} &\omega_{\mathrm{ph}}(^{16}\mathrm{O}) = 308 \pm 3\mathrm{cm}^{-1}, \\ &\omega_{\mathrm{CF}} = 304 \pm 3\mathrm{cm}^{-1}, \\ &V = \ 35 \pm 3\mathrm{cm}^{-1}. \end{aligned} \tag{14}$$

We find a very strong coupling with $V > |\omega_{\mathrm{ph}} - \omega_{\mathrm{CF}}|$ so that second-order perturbation theory indeed does not apply. Our approach to diagonalize the Hamiltonian Eqs. (11) and (12) exactly is therefore justified. As mentioned at the end of Sec. IV, V is the average coupling strength over the Brillouin zone. The fact that we observe the two peaks shows that the phonon band, or at

least that part of it that couples strongly to the CF excitation, is indeed very narrow so that we can approximate it as flat.

Strong confirmation of these parameters arises from the good agreement obtained for the ^{18}O-substituted samples if we only shift ω_{ph} by the expected mass effect [$\omega_{ph}(^{18}O) = \sqrt{16/18}\omega_{ph}(^{16}O)$] and leave the other parameters unchanged:

$$\omega_{ph}(^{18}O) = 290 \pm 3 \text{ cm}^{-1}. \quad (15)$$

We then not only obtain the correct peak positions, but also the different intensity ratio is well reproduced. Γ_{ij} was taken to be 10 cm^{-1} for all i, j and either oxygen isotope.

For elevated temperatures the spectral function is considerably enriched, since many more transitions above, between, and below the low-temperature peaks are involved, leading to a strong broadening. Also the two low-temperature peaks approach each other. Using the parameters mentioned above, we can, up to $\approx$ 150 K, describe the ^{16}O as well as ^{18}O cases equally well (dashed lines in Fig. 9). We let Γ_{ij} increase independently of i and j from 10 cm^{-1} at 10 K to 15 cm^{-1} at 300 K, as expected from $YBa_2Cu_3O_7$ data. This choice is not particularly relevant, since Γ_{ij} is much smaller than the width of the structure given by the variety of different transitions. At room temperature, however, the spectral weight far away from the center is overestimated by the theory.

Two processes might be responsible for this difference.

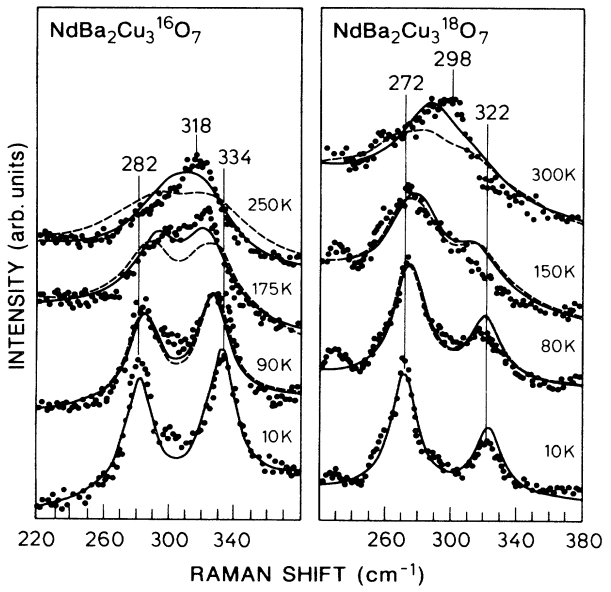

FIG. 9. Raman spectra of the $NdBa_2Cu_3{}^{16}O_7$ and $NdBa_2Cu_3{}^{18}O_7$ ceramic samples as measured (dots) and calculated from Eqs. (10)–(14) without ($\kappa = 0$, dashed lines) and with [$\kappa(^{16}O) = 2.6 \times 10^{-3}$ K^{-1}, $\kappa(^{18}O) = 2.6 \times 10^{-3}$ K^{-1}, solid lines] the inclusion of higher-order effects as described by Eq. (14).

(i) Many more diagrams than those sketched in Fig. 8 are, in principle, allowed and could be relevant. Two-phonon processes might be important, since, e.g., $|n, 0>$ and $|n+2, -j-k>$ have almost the same energy. Anharmonic two-phonon processes as vertex corrections to Fig. 8 should lead to terms proportional to $< u >^4 \sim T^2$ so that a corrected effective matrix element could have the form

$$\tilde{V} = V(1 - (\kappa T)^2), \quad (16)$$

where the sign of the correction term is not clear, *a priori*. Other vertex corrections might play a role as well.[8]

(ii) The effect of phonon dispersion at high temperatures is difficult to estimate. At 300 K part of the spectral function is within the phonon continuum, which has a width of 15 cm^{-1}.[18] The CF component of the participating states might then decay into the continuum (as outlined at the end of Sec. IV), which could lead to a weaker effective coupling than that expected from Eqs. (10)–(13). Clearly, more theoretical work is needed to evaluate this effect quantitatively. In order to keep the matter simple, we approximate this process heuristically also with Eq. (16), the correction term now always being negative.

Using $\kappa = 2.6 \times 10^{-3}$ K^{-1} (which leads to a 50% reduction of $\tilde{V}$ at 300 K), we obtain very good agreement with experiment (Fig. 9, solid lines) even at room temperature. For the ^{18}O sample, the fit was slightly better for $\kappa = 2.1 \times 10^{-3}$ K^{-1}. (Given the complicated dependence of κ on anharmonic and other higher-order processes as well as on the phonon dispersion, it is not surprising that κ varies for different isotopes.)

In particular, the theory of coupled phonon-CF excitations describes the temperature dependence for different isotopes. For ^{16}O, $\omega_{CF} < \omega_{ph}$, and hence the lower peak disappears at elevated temperatures. For ^{18}O, we have $\omega_{CF} > \omega_{ph}$ so that now the higher peak vanishes at 300 K. Also the temperature-dependent isotope effect is described correctly. This has mainly two origins.

(i) At low temperature both peaks correspond to strongly coupled quasiparticles both having only approximately 50% phonon content so that only half the expected isotopic shift is observed. At 300 K, the coupling, and hence the mixing, are much smaller. The phononlike peak, having now much less CF admixture, dominates the spectrum and leads to a complete isotope shift (6%).

(ii) For phonon quantum numbers $n \geq 1$, it is easy to check from Eqs. (11) and (12) that the isotopic shift of the transitions $E_i^{n+1} - E_j^n$ is always $\sqrt{16/18}$, independent of the mixing, although the participating levels E_i^n have shifts that depend on phonon quantum number as well as the mixing. Only the $n = 0$ transitions have just half the shift for large couplings. If at elevated temperatures the $n = 1$ transitions become more important, the $n = 1$ term in Eq. (13) contributes to the full isotopic shift.

A very strong argument for the validity of this model is the observation of a double peak in the CF excitation spectrum as measured by inelastic neutron-scattering by Allenspach *et al.* (Fig. 10). At small momentum transfers, such as those used in their experiment, CF excitation scattering dominates over phonon scattering. So the

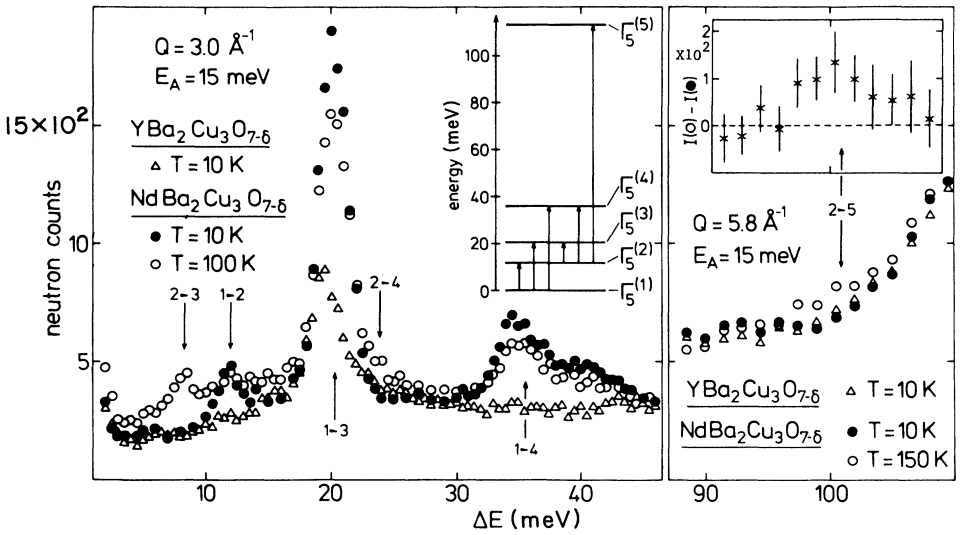

FIG. 10. Inelastic-neutron-scattering spectrum of $NdBa_2Cu_3O_7$ measured by Allenspach *et al.* (Ref. 5) showing the CF-excitation-like component of the coupled excitation at 34.9 and 40.5 meV at 10 K (solid circles) and 100 K (open circles) and for comparison the spectrum of $YBa_2Cu_3O_7$ (triangles), which should have a very similar phononic background but no CF excitations, since it lacks any $4f$ electrons. The inset in the left panel shows the CF level scheme as in Fig. 7 and the symmetry assignment in the orthorhombic group D_{2h} [figure taken from Allenspach *et al.* (Ref. 5).]

intensity of the double peak is entirely due to the CF component, in contrast to our Raman experiment, where only the phonon component contributes. They find frequencies of 34.9 meV = 282 cm^{-1} and 40.5 meV = 326 cm^{-1}, which are the same within the resolution of inelastic neutron scattering as in our experiment. Although Allenspach *et al.* attribute the double peak to "distorted CF excitations" due to oxygen vacancies, it now seems evident that they observe the same structure in their CF spectra that we see in our phononic spectra.

With neutron scattering, one can measure the **k** dependence of the coupled modes, provided that large single crystals are available. If the nondispersive CF band and a weakly dispersive [$\approx$ 15 cm^{-1} (Ref. 18)] phonon band interact, one obtains two renormalized bands that are both weakly dispersive. In contrast to Raman scattering, which practically only detects the phonon component of the coupled excitations at $\mathbf{k} \approx \mathbf{0}$, neutron scattering is sensitive to the CF as well as the phonon component, the respective cross sections depending also on the wave vector **k**. Using neutron scattering without **k** resolution one thus obtains only an average of both bands over the Brillouin zone. For $CeAl_2$ it was observed that Raman scattering[20] and inelastic-neutron-scattering spectra[21] do not coincide, even for scattering by phonons at the Γ point, and have different temperature dependences. This behavior was not fully understood. It will therefore be of interest to investigate thoroughly the phonon and CF neutron-spectra as a function of wave vector **k** as well as of temperature also for $NdBa_2Cu_3O_{7-\delta}$.

We expect the neutron-scattering intensities to be proportional to p_1, i.e., to decrease with increasing temperature, since the inelastic neutron scattering can only excite a given CF excitation if the participating $4f$ configuration is in its ground state. Allenspach *et al.* only measured at 10 and 100 K, where $p_1 = 0.5$ and 0.369, respectively, so that we expect a 26% decrease in intensity. This is indeed what they observed (Fig. 10).

For the sake of completeness, we now discuss the parameters necessary to fit the data for the $NdBa_2Cu_3\,{}^{16}O_7$ crystal and for the $NdBa_2Cu_3\,{}^{16}O_6$ ceramic sample. We see in Fig. 2 that the low-temperature intensity ratio of the doublet in the case of the $NdBa_2Cu_3\,{}^{16}O_7$ crystal is somewhat different from that in the ceramic sample (Fig. 3) of nominally the same composition. We therefore have to assume a larger difference $\omega_{ph} - \omega_{CF}$ in order to have a smaller coupling. The data can then be well described (Fig. 11, left panel) by

$$\begin{aligned} &\omega_{ph}(^{16}O) = 308 \pm 3 \text{ cm}^{-1}, \\ &\omega_{CF} = 296 \pm 3 \text{ cm}^{-1}, \\ &V = 39 \pm 3 \text{ cm}^{-1}, \\ &\kappa = 2.3 \times 10^{-3} \text{ K}^{-1}. \end{aligned} \tag{17}$$

We suspect the different parameters are due to different preparation conditions. In particular, it is known that Nd also partially occupies the Ba sites,[22] the concentration depending on sample preparation. This might lead to a different crystal field.

For $NdBa_2Cu_3O_6$, the situation seems to be more complicated. At room temperature, we observe (Fig. 4) only the upper mode, which is therefore the phononlike quasiparticle. In agreement with our expectations, it shifts by 16 cm^{-1} to higher energies when the sample is cooled to low temperature. At the same time, the lower CF-

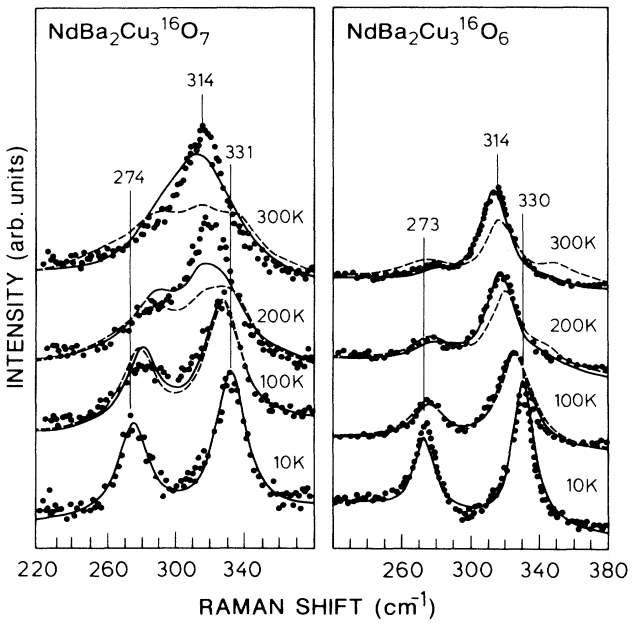

FIG. 11. Raman spectra of the $NdBa_2Cu_3{}^{16}O_7$ single crystal (left panel) and the $NdBa_2Cu_3{}^{16}O_6$ ceramic samples (right panel) as measured (dots) and calculated from Eqs. (10)–(14) using parameters as mentioned in the text without ($\kappa = 0$, dashed lines) and with (solid lines) the inclusion of higher-order effects as described by Eq. (16).

like peak appears. However, the frequency of the CF-like peak seems to be almost independent of temperature. This observation cannot be explained within our model if we assume the unperturbed frequencies to be temperature independent, as we did above. One usually expects an increase of $\omega_{\rm ph}$ by only a few wave numbers with decreasing temperature; here, however, we have to assume $\omega_{\rm CF}$ to decrease with increasing temperature in order to describe well our results, a fact which, however, is not incompatible with an additional anharmonic renormalization mechanism. The 10-K spectrum, as explained above, already determines V, $\omega_{\rm ph}(10\ {\rm K})$, and $\omega_{\rm CF}(10\ {\rm K})$. We find

$$\begin{aligned} &\omega_{\rm ph}({}^{16}{\rm O}) = 311 \pm 3\ {\rm cm}^{-1}, \\ &\omega_{\rm CF} = 292 \pm 3\ {\rm cm}^{-1}, \\ &V = 38 \pm 3\ {\rm cm}^{-1}. \end{aligned} \tag{18}$$

It was shown by Furrer *et al.*[23] for the case of $ErBa_2Cu_3O_{7-\delta}$ that the crystal-field levels can depend significantly on the oxygen content, since a change of δ induces a change in the charge distribution. It is therefore no surprise that $\omega_{\rm CF}$ is lower than in the fully oxygenated ceramic sample [Eq. (14)]. In order to describe properly our spectra, we have to assume the following dependence of $\omega_{\rm CF}$ on temperature (Fig. 11, right panel):

$$\begin{aligned} &\omega_{\rm CF}(10\ {\rm K}, {\rm O}_6) = 292\ {\rm cm}^{-1}, \\ &\omega_{\rm CF}(100\ {\rm K}, {\rm O}_6) = 288\ {\rm cm}^{-1}, \\ &\omega_{\rm CF}(200\ {\rm K}, {\rm O}_6) = 284\ {\rm cm}^{-1}, \\ &\omega_{\rm CF}(300\ {\rm K}, {\rm O}_6) = 280\ {\rm cm}^{-1}, \\ &\kappa = 3.0 \times 10^{-3}\ {\rm K}^{-1}. \end{aligned} \tag{19}$$

Here, we had to choose $\Gamma_{ij} = 10\ {\rm cm}^{-1}$ independent of temperature. It would be of interest to confirm this interpretation by the corresponding measurement of $\omega_{\rm CF}$ as a function of temperature and oxygen content by inelastic neutron scattering.

VII. POLARIZATION DEPENDENCE OF THE O(4) PEAK

We finally discuss briefly some unusual properties of the phonon spectra (Fig. 1). The highest peak, usually assigned to the z-directed motion of the apical oxygen atom O(4), has different energies in the $x(zz)\bar{x}$ and and $z(xx)\bar{z}$ spectra, i.e., 520 and 555 $\rm cm^{-1}$, respectively. This feature has also been observed by Yoshida *et al.*[1] The spectrum of the ceramic sample, however, only exhibits a strong and narrow peak at 516 $\rm cm^{-1}$ (not shown in the figure). The 555-$\rm cm^{-1}$ structure does not follow any polarization selection rules, while the 520-$\rm cm^{-1}$ peak seems to appear only in $x(zz)\bar{x}$ configuration. We believe that only the lower frequency corresponds to the true A_{1g} O(4) phonon and that the broad distribution observed in $z(xx)\bar{z}$ represents rather a phonon density of states: Only the lower frequency fits into a plot of the phonon frequency versus rare earth atomic radius.[24] Similar observations have also been made on $PrBa_2Cu_3O_7$, where the highest phonon mode has a smaller width and a lower frequency for a ceramic sample[25] [where the $x(zz)\bar{x}$ component dominates] than for $z(xx)\bar{z}$ in a single crystal.[26] This may be an indication that Pr and Nd are already nearly too big to form the 1:2:3 structure. It is known[22] that therefore in these two cases the rare-earth ions tend to partially occupy also the Ba site, hence breaking the translational symmetry of the lattice and therefore **k** conservation. While the $x(zz)\bar{x}$ Raman activity depends almost entirely on the deformation potentials connected with the stretching of the O(4)–Cu(1) bond,[3] which does not feel the Ba site significantly, the smaller $z(xx)\bar{z}$ activity is caused by an interplay of a large number of interband transitions, of which many have Ba orbital content.[3] Hence, only in $z(xx)\bar{z}$ configuration, we expect a significant effect of the disorder, in agreement with the experiment. The fact that the mode has in $x(zz)\bar{x}$ configuration a higher frequency than in the spectra of Yoshida *et al.*[1] probably just reflects the higher oxygen content in our sample. A more detailed analysis, as well as more experimental evidence, will be published elsewhere.[27]

The relatively high frequencies of the Ba A_{1g} (142 $\rm cm^{-1}$ at 10 K) and Cu(2) A_{1g} (172 $\rm cm^{-1}$) phonons in the single crystal are another surprising observation. This is much higher than that for our ceramic sample (115/152 $\rm cm^{-1}$ at 10 K, no figure) and higher than for the 1:2:3 materials containing rare earths of similar size like Pr [118/149 (Ref. 25) and 147 (Ref. 28) $\rm cm^{-1}$] and Sm [151 $\rm cm^{-1}$ (Ref. 28)]. On the other hand the frequencies of the other phonons do not deviate that drastically from the expectations, indicating that there might exist peculiarities in the interatomic distances which, to our knowledge, have not been reported so far.

VIII. CONCLUSION

In this paper, we demonstrated that the coupling of the B_{1g} phonon to a CF excitation of the same symmetry leads to a double peak in neutron as well as Raman scattering spectra. We presented a model that is able to describe our observations well. Our considerations are supported by a detailed analysis of the dependence of the Raman spectra on temperature, isotopic substitution, oxygen content, and laser wavelength. We point out that the double-peak feature could have a different temperature dependence in neutron- and Raman-scattering spectra and encourage clarifying neutron-scattering measurements. We obtain the parameters of the coupling strength $V = 35$ cm^{-1} (which should be compared to future calculations, which should be easy to perform with a standard CF code), and the unperturbed frequencies $\omega_{\rm ph} = 308$ cm^{-1} and $\omega_{\rm CF} = 304$ cm^{-1}. Higher-order processes [leading to Eq. (16)] should be further investigated in the future.

Finally, we showed that the substitution of Ba by rare-earth atoms in $PrBa_2Cu_3O_7$ and $NdBa_2Cu_3O_7$ induces a broad band in the $z(xx)\bar{z}$ spectra around 555 cm^{-1} and a sharp peak in the $x(zz)\bar{x}$ spectrum near 516 cm^{-1}; only the latter corresponds to the O(4) Γ-point frequency.

ACKNOWLEDGMENTS

We thank B. Friedl and C. Thomsen for calling our attention to this material, P. Murugaraj for the preparation of some of the samples, O. Buresch for the chemical analysis, R. Kremer for the susceptibility measurements, C.K. Loong for an illuminating telephone call, and W. Kress for a critical reading of the manuscript. Thanks are also due to H. Hirt, M. Siemers, and P. Wurster for expert technical help. We gratefully acknowledge financial support from the Bundesminister für Forschung und Technologie and the European Community.

[1] M. Yoshida, S. Gotoh, T. Takata, N. Koshizuka, and S. Tanaka, Phys. Rev. B **41**, 11 689 (1990).
[2] R. Liu, C. Thomsen, W. Kress, M. Cardona, B. Gegenheimer, F.W. de Wette, J. Prade, A.D. Kulkarni, and U. Schröder, Phys. Rev. B **37**, 7971 (1988).
[3] E.T. Heyen, S.N. Rashkeev, I.I. Mazin, O.K. Andersen, R. Liu, M. Cardona, and O. Jepsen, Phys. Rev. Lett. **65**, 3048 (1990).
[4] E.T. Heyen, R. Wegerer, and M. Cardona, Phys. Rev. Lett. **67**, 144 (1991).
[5] P. Allenspach, A. Furrer, P. Bruesch, and P. Unternaehrer, Physica B **156-157**, 864 (1989).
[6] M. Loewenhaupt, B.D. Rainford, and F. Steglich, Phys. Rev. Lett. **42**, 1709 (1979).
[7] P. Thalmeier and P. Fulde, Phys. Rev. Lett. **49**, 1588 (1982).
[8] P. Thalmeier, J. Phys. C **17**, 4153 (1984).
[9] P. Murugaraj, J. Maier, and A. Rabenau, Solid State Commun. **71**, 167 (1989).
[10] C.A. Morrison and R.P. Leavitt, in *Handbook on the Physics and Chemistry of Rare Earths*, edited by K.A. Gschneidner and L. Eyring (North-Holland, Amsterdam, 1982), Vol. 5.
[11] G.F. Koster, in *Solid State Physics*, edited by F. Seitz and F. Turnbull (Academic, New York, 1957), Vol 5.
[12] K.R. Lea, M.J.M. Leask, and W.P. Wolf, J. Phys. Chem. Solids **23**, 1381 (1962).
[13] P. Fulde, in *Handbook on the Physics and Chemistry of Rare Earths*, edited by K.A. Gschneidner and L. Eyring (North-Holland, Amsterdam, 1979), Vol. 2, pp. 305ff, and references therein.
[14] G.L. Goodman, C.-K. Loong, and L. Soderholm, J. Phys. Condens. Matter **3**, 49 (1991).
[15] P. Allenspach, A. Furrer, and F. Hulliger, Phys. Rev. B **39**, 2226 (1989).
[16] A. Furrer, P. Bruesch, and P. Unternahrer, Phys. Rev. B **38**, 4616 (1988).
[17] P. Allenspach, U. Staub, A. Furrer, E. Kaldis, J. Karpinski, S. Rusiecki, and H. Blank (unpublished).
[18] Pintschovius *et al.* (unpublished).
[19] M. Cardona, in *Light Scattering in Solids I*, edited by M. Cardona, 2nd ed. (Springer-Verlag, Heidelberg, 1983).
[20] G. Güntherodt, E. Zirngiebl, S. Blumenröder, A. Jayaraman, B. Batlogg, M. Croft, and E. Melczer, J. Magn. Magn. Mater. **47/48**, 315 (1985).
[21] W. Reichardt and N. Nücker, J. Phys. F **14**, L135 (1984).
[22] S.Takekawa, H. Nozaki, Y. Ishizawa, and N. Igi, Jpn. J. Appl. Phys. **26**, L2076 (1987).
[23] A. Furrer, P. Allenspach, J. Mesot, U. Staub, H. Blank, H. Mutka, C. Vettier, E. Kaldis, J. Karpinski, S. Rusiecki, and A. Mirmelstein (unpublished).
[24] M. Cardona, R. Liu, C. Thomsen, M. Bauer, L. Genzel, W. König, A. Wittlin, U. Amador, M. Barahona, F. Fernández, C. Otero, and R. Saéz, Solid State Commun. **65**, 71 (1988).
[25] H.B. Radousky, K.F. McCarty, J.L. Peng, and R.N. Shelton, Phys. Rev. B **39**, 12 383 (1989).
[26] R. Liu (private communication).
[27] R. Wegerer, E.T. Heyen, and M. Cardona (unpublished).
[28] H.J. Rosen, R.M. McFarlane, E.M. Engler, V.Y. Lee, and R.D.Jacowitz, Phys. Rev. B **38**, 2460 (1988).